GDCh

Research Articles

Angewandte Chemie
International Edition
www.angewandte.org

How to cite: *Angew. Chem. Int. Ed.* **2023**, *62*, e202304163
doi.org/10.1002/anie.202304163

Check for updates

Reaction Mechanisms

Mechanisms of Cysteine-Lysine Covalent Linkage—The Role of Reactive Oxygen Species and Competition with Disulfide Bonds**

Jin Ye, Sophia Bazzi, Tobias Fritz, Kai Tittmann, Ricardo A. Mata, and Jon Uranga

Abstract: Recently, a new naturally occurring covalent linkage was characterised, involving a cysteine and a lysine, bridged through an oxygen atom. The latter was dubbed as the *NOS bond*, reflecting the individual atoms involved in this uncommon bond which finds little parallel in lab chemistry. It is found to form under oxidising conditions and is reversible upon addition of reducing agents. Further studies have identified the bond in crystal structures across a variety of systems and organisms, potentially playing an important role in regulation, cellular defense and replication. Not only that, double NOS bonds have been identified and even found to be competitive in relation to the formation of disulfide bonds. This raises several questions about how this exotic bond comes to be, what are the intermediates involved in its formation and how it competes with other pathways of sulfide oxidation. With this objective in mind, we revisited our first proposed mechanism for the reaction with model electronic structure calculations, adding information about the reactivity with alternative reactive oxygen species and other potential competing products of oxidation. We present a network with more than 30 reactions which provides one of the most encompassing pictures for cysteine oxidation pathways to date.

Introduction

Cysteine (Cys) residues are well-known for their rich redox activity.[1] This includes the formation of disulfide bonds by oxidation of two neighbouring Cys, a staple post-translational modification in proteins. These bridges play a key role in protein folding, regulation and stability.[2–4] Recently, a new covalent cross-link between Cys and lysine (Lys) residues, which are linked via an oxygen atom, has been characterised.[5] This linkage, first discovered in the Transladolase of *Neisseria gonorrhoeae*, was termed NOS bridge and has been subsequently shown to occur in a wide variety of proteins, e.g. the main protease of SARS-CoV-2 (M^{pro}),[6,7] with very diverse implications for catalytic and regulatory mechanisms.[6,8,9] A recent study[10] has also shown how this crosslink can be generated with the use of synthetic fluorescent proteins.

Surprisingly, this bond forms non-catalytically under oxidative conditions and the reduced Cys and Lys residues can be fully recovered under the action of reducing agents. A recent experiment has demonstrated the functional reversibility of NOS in the range of 0.1–1 mM H_2O_2, concentrations which are expected under oxidative stress.[11] At supraphysiological concentrations of H_2O_2, 20 mM, NOS bridges were no longer detected due to over-oxidation.[12] The formation of such a cross-link requires the oxidation of both Cys and Lys residues. Cys residues are broadly known to oxidise through the thiol moiety leading to a wide variety of oxidation products such as the thiyl radical, the disulfide bond or the sulfenic acid under mild oxidation conditions or the sulfinic acid under higher oxidant concentrations.[13–19] In this vein, an antioxidizing character is commonly attributed to the thiol moiety, due to its ability to quench oxidizing species.[20] A clear biological example being the Glutathione, a tripeptide found in different organisms, protecting them against oxidation.[21] On the other hand, Lys residues are less susceptible to oxidation and in case of oxidation, the formation of carbonyl groups have been reported.[22–24] It is therefore surprising to observe a cross-linker formed by these pair of residues. Still, the formation of single NOS bridges has now been confirmed after a long-standing discussion.[5,25–28] These observations have expanded, with further oxidation of the amino moiety of the Lys being confirmed. A double NOS bond involving two Cys and a Lys (SONOS) has been reported by different research groups in M^{pro}.[6,7]

There is so far very little information about the potential mechanism of formation. For the reaction in vivo, hydrogen peroxide (H_2O_2) or the superoxide anion radical ($O_2^{\bullet-}$) will

[*] J. Ye, S. Bazzi, T. Fritz, R. A. Mata, J. Uranga
Institute for Physical Chemistry, Georg-August Universität Göttingen, Tammannstraße 6, D-37077 Göttingen (Germany)
E-mail: juranga@gwdg.de

K. Tittmann
Department of Molecular Enzymology, Göttingen Center of Molecular Biosciences, Georg-August University Göttingen, Göttingen (Germany)

K. Tittmann
Department of Structural Dynamics, Max-Planck-Institute for Multidisciplinary Sciences, Göttingen (Germany)

Angew. Chem. Int. Ed. **2023**, *62*, e202304163 (1 of 10)

© 2023 The Authors. Angewandte Chemie International Edition published by Wiley-VCH GmbH

be likely involved as major biological redox signalling agents.[29] The resolved X-ray structure of the reduced Transladolase from *Neisseria gonorrhoeae* (PDB code 6ZWF) showed a molecular oxygen in the vicinity of the bridging Cys and Lys residues, suggesting that this pocket could potentially bind the aforementioned reactive oxygen species (ROS). This same study showed that there were no significant conformational changes in the system between oxidised and reduced states (Figure 1). It has also been observed that NOS bonds can be formed both in the presence of molecular oxygen and hydrogen peroxide in solution, the latter being somewhat faster.[5] The exact identity and the breadth of ROS which can bring about the reaction are unknown, given that the chemistry of ROS in water is quite intricate.[30] Take for example the recent discovery of spontaneous hydrogen peroxide formation in water microdroplets.[31] We decided to focus foremost on three potential agents—hydrogen peroxide,[32] triplet and singlet molecular oxygen[33]—which we believe will be representative. We extended this list including obvious suspects such as the superoxide anion radical and the derivatives that may arise from the decomposition of hydrogen peroxide, e.g. the hydroxyl radical ($^\bullet$OH), the hydroperoxyl radical ($^\bullet$OOH) and the hydronium radical ($^\bullet$H$_3$O). The resulting unstable and easily-reactive radical species generated by the hydrogen peroxide decomposition would readily react with nearby residues, owing to their low kinetic barriers and thermodynamic instability.[17,24,34,35] On the homolytic dissociation of H$_2$O$_2$, the formation of $^\bullet$OH was reported to be around 50 kcal mol^{-1} in gas phase,[36] and in water the bond was shown to be 2–5 kcal mol^{-1} weaker.[37] Recently, calculations have put forward that in solution hydrogen peroxide can dissociate to $^\bullet$OH or $^\bullet$OOH and

$^\bullet$H$_3$O with activation barriers of 11.3 kcal mol^{-1} and 8.2 kcal mol^{-1} respectively, making these species somewhat accessible.[38] The study of the decomposition mechanism of H$_2$O$_2$ in water and the review of these values is beyond the scope of the current work, as we will focus primarily on the oxidation of the target residues. Albeit pertinent, it is extremely intricate to clearly identify the ROS responsible for the reaction, as a multitude of intermediates can form in solution. The intermediates considered in this study should be viewed as potential radical species which promote the oxidation of Cys and Lys residues. Overall, the atomistic mechanism of the oxidation of Cys and Lys residues in the framework of NOS formation is not yet understood.[39] An electronegative atom such as oxygen bridging nitrogen and sulfur is somewhat counterintuitive, and indeed there are few examples in lab chemistry for this type of bond.[40,41] This work is devoted to shed light into the reaction mechanism for the formation of the cross-link, exploring different oxidizing agents and intermediates. Particular focus is given to the question of how NOS formation proves to be competitive in relation to other oxidizing pathways of Cys, especially for the formation of the disulfide bond.

Results and Discussion

With the aim of identifying potential intermediate states and the oxidant chemical species that lead to the formation of the NOS and SONOS, first we analyse the reduction potentials of the thiol/thiolate and the amine moieties, as well as the oxidant species. Thereafter, we present the reaction mechanisms for the formation of the oxidised intermediate with different oxidants and finally we present the reaction mechanism for the NOS and SONOS formation.

Geometry optimizations and frequency calculations were performed using the Gaussian16 software package.[42] We have used Density Functional Theory (DFT), namely the B3LYP functional[43,44] together with the def2-SVPD basis set[45,46] for geometry optimizations. All calculations included Grimme's D3 dispersion correction[47] with Becke-Johnson damping function[48] and the SMD continuum model[49] with the permittivity of water. Transition state searches were carried out by an in-house nudged elastic band code.[50] For some cases, it was necessary to manipulate the structures to obtain sensible starting paths or structures. The determination of whether the identified structures are minima or transition states was carried out by analytically differentiating gradients to obtain harmonic vibrational frequencies. The connection between transition states and intermediates was verified by displacing the molecular geometry along the imaginary mode and relaxing the structures. Subsequently, the frequencies obtained were used to evaluate the zero-point vibrational energy (ZPVE) and thermal vibrational corrections to the Gibbs free energy in the harmonic oscillator approximation at a temperature of 298 K. Grimme's quasi-harmonic approximation was applied for vibrations under 100 cm^{-1} at 298.15 K to correct the vibrational entropies using the Goodvibes program.[51,52] The
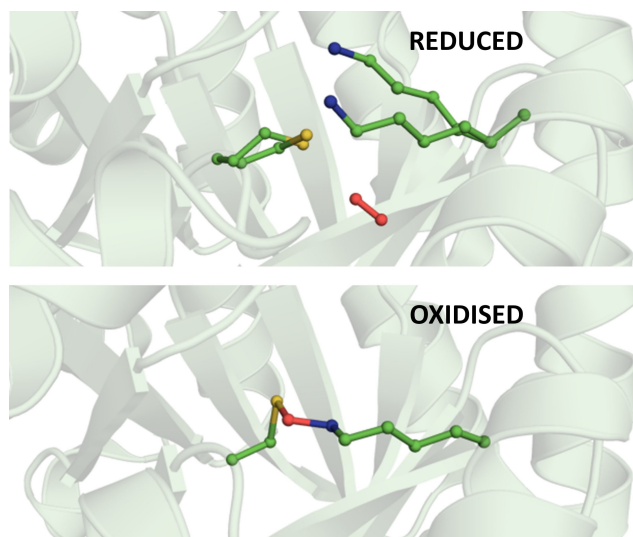

Figure 1. X-ray crystallography images of both reduced and oxidised forms of *Neisseria gonorrhoeae* transaldolase. The top image (PDB code: 6ZWF) represents the reduced form with a distance of R(C_α–C_α) = 9.2–9.4 Å, showing two conformations for both residues above 20% occupancy after refinement. The bottom image (PDB code: 6ZX4) illustrates the oxidised form with a distance of R(C_α–C_α) = 9.3 Å.

electronic energies were refined using the def2-TZVPD basis set. The barriers were estimated on the basis of classical transition state theory. For all states with unpaired electrons, the unrestricted formalism was applied, as well as in the search for broken-symmetry states. The topological analysis was performed with Multiwfn 3.8 software package.[53] The atomic charges were derived using the Hirshfeld population analysis,[54] the spin densities and the bond orders were computed using the Fuzzy partition scheme.[55,56]

Calculation of chemical reactions and benchmarking

With the aim of evaluating the performance of the theoretical method, we have selected different molecules whose experimental relative enthalpies, Gibbs free energies and reduction potentials were documented. We make use of dissociation and H atom abstraction reactions (see Table S1) as well as reduction potentials (see Table S2) to benchmark our approach. We have employed the value of $-271.91 \, \text{kcal mol}^{-1}$ for the (H^+),[57] and obtained a value of $-98.72 \, \text{kcal mol}^{-1}$ for (e^-) using the standard hydrogen electrode (SHE) as reference (0.0), computing the values for the hydrogen molecule with the already mentioned QM protocol. Overall, the mean absolute deviation (MAD) values indicate that for the explored chemical reactions, the deviations of ΔH^0 and ΔG^0 are within $2.5 \, \text{kcal mol}^{-1}$ whereas for the reduction potentials the deviations are within $0.09 \, \text{V}$. These results show that the level of theory would be adequate for the study of the reactive processes targeted.

Choice of model systems

So far, observation of NOS or SONOS bond formation shows little dependence on the environment.[6] When it was first reported in the transaldolase enzyme of *Neisseria gonorrhoeae*,[5] the possible action of a near-lying glutamic acid residue (E93) was considered, but ultimately not confirmed. With the observation of the bond in a wide variety of locations, hydrophobic to hydrophylic, exposed or buried, intra- and intermolecular, there is little in common between the identified neighbouring residues, strongly suggesting that the general mechanism of formation does not require the presence of a third specific reaction partner.
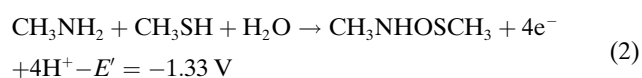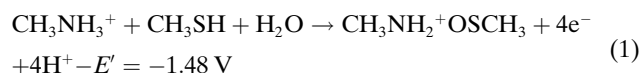
Therefore, we believe it is justified to use a simple model to calculate and compare the different reaction paths. It should be noted that whenever charges are formed, the stability of the intermediates or transition states might be more strongly impacted by local electrostatic potentials. However, there is no practical way to condense the information of the dozens of confirmed systems for NOS formation into a usable model. On the plus side, the inherent simplicity of the system used does allow for a comparison of different competing mechanisms in a rather balanced way, doing away with steric constraints and potential bias in system preparation.

The Cys and Lys residues are included truncating them at the backbone C_α atoms. The latter carbon atoms are saturated with hydrogens and kept constrained to their crystallographic position during the optimizations. The reaction mechanism involving the NOS formation is modelled fixing the C_α's to the *Neisseria gonorrhoeae* transaldolase (PDB code 6ZX4) data,[5] whereas the reaction mechanism for the formation of the SONOS is modelled using the M$^{\text{pro}}$ of SARS-CoV-2 (PDB code 7JR4) coordinates. Without these constraints, the two residues could aggregate and/or exhibit large motions during the reaction pathway modelling. The use of observed C_α positions is a minimum condition imposed on the calculations to avoid unphysical artefacts of the cluster model.

Reduction and oxidation potentials

The propensity to oxidation of different chemical entities is analysed through their reduction/oxidation potentials. By observing these values alone, the thermodynamic propensity for a reaction to happen can be readily estimated. In Figures S2 and S3 the computed oxidation potentials of probable intermediates in the NOS bond formation are shown. It can be observed that the oxidation of the thiol/thiolate moiety leads to lower oxidation potentials when compared to the amino moiety, thereby making the former more prone to oxidation, as it is generally known. The results follow chemical common sense that in the first stage of the oxidation, the thiol moiety is the one likely to be oxidised.

A variety of oxidation products can be formed departing from the thiol/thiolate moiety. The thiyl radical, sulfenic and sulfinic acids lead to the lowest values and are therefore thermodynamically the most favourable oxidation products. However, it should be noted that the formation of the sulfinic acid is known to be a thermodynamic trap. Due to its high thermodynamic stability the reaction would be at a dead end.[5] In order to reduce this product, one would require some sort of catalysis, which in nature can be achieved by Cys sulfinic acid reductases.[58] This implies that sulfinic acid cannot play a role as an intermediate and that a species at a lower oxidation state is required. This would include species such as the thiyl radical, the sulfenic acid or the thio-(hydro)peroxy acid, which would allow the reaction to proceed, ultimately leading to the formation of the NOS bond. Further oxidation reactions of the already oxidised thiol/thiolate and amine moieties are also shown in Figures S2 and S3. It can be seen that the thio-(hydro)peroxy acid is the most unstable species (potentials below $-1.6 \, \text{V}$). Once formed it can be reduced to the thiyl radical or sulfenic acid, while potentially oxidising nearby chemical entities.

$$\text{CH}_3\text{NH}_3^+ + \text{CH}_3\text{SH} + \text{H}_2\text{O} \rightarrow \text{CH}_3\text{NH}_2^+\text{OSCH}_3 + 4\text{e}^- \\ +4\text{H}^+ - E' = -1.48 \, \text{V} \tag{1}$$

$$\text{CH}_3\text{NH}_2 + \text{CH}_3\text{SH} + \text{H}_2\text{O} \rightarrow \text{CH}_3\text{NHOSCH}_3 + 4\text{e}^- \\ +4\text{H}^+ - E' = -1.33 \, \text{V} \tag{2}$$

We have then considered potential oxidant agents (Figure S4), in conjunction with Equations (1) and (2), in order to obtain an estimate for the full redox process of NOS formation. It is interesting to note that the NOS formation from the amine and thiol moieties is possible with hydrogen peroxide (H_2O_2), as it was reported in the experimental assays.[5] Moreover, the potential for hydrogen peroxide reduction closely matches the potential for NOS formation, in accordance with the reported reversibility of the bond. The hydroxyl radical (•OH) displays the highest reduction potential (2.25 V) among the considered oxidants and is able to oxidise most of the chemical species under study. This value should be considered with care as this species will likely further react with water. Ground state molecular oxygen on the other hand shows the lowest reduction potential value (0.81 V). Hence, the oxidation with this species leading to the formation of a NOS bond would not be a spontaneous process. Having considered the different redox potentials of the species under study, and the thermochemistry of NOS bond formation, we now look into the formation of potential intermediates along the reaction pathway leading to the NOS cross-link. We introduce the first reaction pathway results, including also kinetic considerations.

Formation of sulfenic acid

Sulfenic acid is known to be formed upon the thiol oxidation in the presence of H_2O_2.[19] The reduction potentials show that the formation of such a chemical entity is a thermodynamically favoured oxidation process and it is herein considered as a potential intermediate in the formation of the NOS bond. The formation of such intermediate is further examined in Figure 2 (a), where its formation upon the oxidation of the thiol/thiolate with H_2O_2 is shown. For completeness, we have also considered the oxidation of the amine moiety. It is well known that the latter is less prone to oxidation than the thiol moiety, see Figure S3. This observation is clear in the calculation results. The oxidation of the amine moiety has a higher associated activation energy and the formed oxidised product is thermodynamically less favored when compared to the oxidation of the thiol, while all the oxidation products are observed to be exergonic processes. The caveat of the sulfenic acid intermediate is that its further oxidation leads to the formation of the thermodynamically very stable sulfinic acid with a low kinetic barrier (7.0 kcal mol⁻¹), shown in Figure 2 (b), arriving at a reaction dead-end. Therefore, the employed concentration of the oxidant species could be a crucial aspect, otherwise one will overoxidise the thiol/thiolate species leading to sulfinic acid formation.

Formation of thio-(hydro)peroxy acid

We have also considered the thio-(hydro)peroxy acid as a potential intermediate candidate. Note that the reduction potential is now higher than for the sulfenic (1.00–1.30 V)
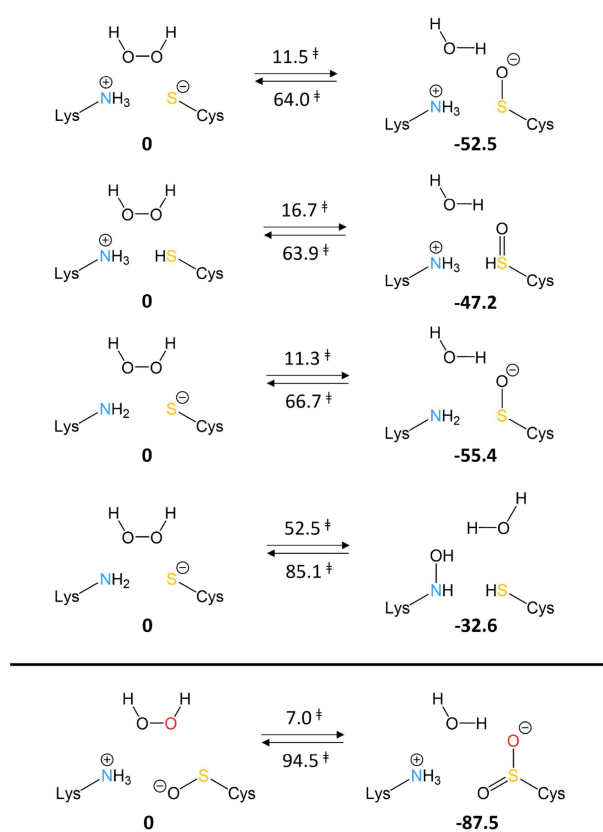

Figure 2. The computed oxidation reaction free energies (kcal mol⁻¹) for (a): the formation of the sulfenic acid in different protonation states and the oxidation of the amine moiety and (b): the formation of the sulfinic acid departing from the sulfenic acid.

and sulfinic (0.70–0.90 V) acids, but similar to the thiyl radical formation, about 1.60 V. Its dissociation could lead to the formation of the sulfenic acid, while at the same time, oxidising any residue nearby. Moreover, the extended "arm" of the peroxy moiety would allow to reach the neighbouring Lys residue, establishing contact between the residues prior to covalent bond formation. Herein, the formation of the thio-(hydro)peroxy acid species is considered, taking into account probable oxidant agents, present in the experimental assays. This can be seen in Figure 3, where the explored pathways for the formation of the thio-(hydro)peroxy acid from a thiol moiety are schematically represented.

Generation with singlet oxygen. The first excited state of molecular oxygen is a singlet, and can readily oxidise a variety of compounds, being commonly viewed as biologically toxic.[59] It can be generated in large quantities through UV light and an organic photosensitizer.[60] It is longer lived in solution than other ROS, so we deemed it of interest how it could be involved in NOS formation.

Figure 3 schematically represents the different reaction pathways we computed to form the thio-(hydro)peroxy acid. For the reactions involving singlet oxygen (the first step in pathways (a) and (b)) caution is advised. We opted for consistency of the different paths to make use of unrestricted Kohn–Sham (UKS). However, it is well-known that the singlet oxygen is severely affected by multireference
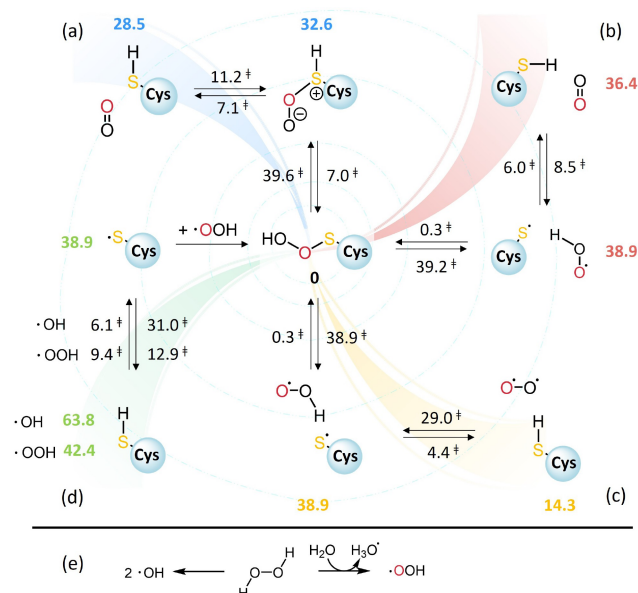
Figure 3. The various computed reaction pathways involved in the formation of SOOH, with corresponding energy values (in black) along the arrows denoting the activation barriers in their respective directions. The energies (in colors consistent with the spiral arm) adjacent to the compounds represent the relative energies of intermediates and reactants, referenced to the thio-(hydro)peroxy acid species in the center. It should be noted that Lys is also implicated but not featured in the image. The pathways include: (a) thiol oxidation with singlet oxygen directly attacking the sulfur atom, (b) thiol oxidation with singlet oxygen attacking the S—H bond, (c) oxidation with triplet oxygen attacking the hydrogen, (d) oxidation with hydrogen peroxide where hydrogen atom transfer (via H•, HO•, or HOO• depending on HOOH dissociation) is succeeded by the recombination of S• and HOO•, and (e) radical dissociation pathways of hydrogen peroxide.[38]

effects. The two barriers are, therefore, expected to carry significant errors. To give an idea of the potential barrier magnitude, we adopt the strategy suggested by Mullinax et al.,[61] and compare the result to the UKS value. The latter strategy consists of carrying out single points in the triplet state reactant, with an added correction of 22.5 kcal mol^{-1}. The barriers of the singlet state molecular oxygen using the unrestricted method are 23.7 and 21.0 kcal mol^{-1} for (a) and (b) respectively (both compounds have a $\langle S^2 \rangle$-value of about 1.00). Using the correction to the triplet state, these barriers change to 11.2 and 8.5 kcal mol^{-1}. The absolute magnitude changes dramatically, again emphasising that these values are tentative at best. But the relative trend is maintained. Pathway (b) appear to be the most preferred mechanism in forming thio-(hydro)peroxy acid when the singlet oxygen attacks the proton of the thiol group. The energy barrier for the attack by a singlet oxygen at the lone electron pair of sulfur, pathway (a), is slightly higher. The benefits of pathway (b) are further enhanced by the subsequent step, which involves a recombination of the intermediary radicals with a barrier of only 0.3 kcal mol^{-1}. On the other hand, the intermediate in pathway (a) would have to go through a barrier of 7.0 kcal mol^{-1} to befall the proton transfer. It

should be noted that beyond the two mentioned reactions we did not observe any spin contamination in the stationary points computed.

Overall, the formation of the intermediates and products is observed to be an exergonic process in all cases, such that the final distribution and concentrations should primarily depend on the activation barriers.

Generation with triplet oxygen. Molecular oxygen is a triplet species in its ground state. Although thermochemically not very stable, it poses significant kinetic barriers for reaction with organic compounds. The oxidation of the thiol moiety with this oxidant leads to a barrier of about 30 kcal mol^{-1} (pathway (c) in Figure 3) and thus leaves little chance for the reaction to proceed when compared to the low kinetic barrier in the backward direction. On the other hand, the reaction intermediate in this mechanism is observed to be endergonic, by about 25.0 kcal mol^{-1}, and so it can be concluded that the oxidation with triplet oxygen is not a favoured process.

Generation with hydrogen peroxide. Hydrogen peroxide has been one of the reactants used to push the equilibrium to the NOS formation.[5] H_2O_2 is a complex oxidant entity which can be decomposed into other different ROS. In order to take this into account, in Figure 3 path (d) we show the oxidation of the thiol moiety, leading to thiyl radical, with hydroxyl and hydroperoxyl radicals that can be formed departing from H_2O_2, as shown in Figure 3 path (e).

The hydroperoxyl radical exhibits a higher kinetic barrier (9.4 kcal mol^{-1}) and leads to a thermodynamically less favourable intermediate (-3.5 kcal mol^{-1}). The hydroxyl radical has a lower activation barrier (6.1 kcal mol^{-1}) but leads to the formation of a thermodynamically much more favoured intermediate (-24.9 kcal mol^{-1}). We have considered the reaction with the hydrogen atom, which leads to the lowest activation barrier (0.4 kcal mol^{-1}) and an exergonic formation of products (-19.7 kcal mol^{-1}). However, we failed to find the transition state of thiol reacting with the hydronium radical, which is the more realistic existing form of the hydrogen atom in aqueous solution. Overall, the formation of the thiyl radical with the studied radical species shows low kinetic barriers and leads to thermodynamically favoured values. The newly formed thiyl radical would thereafter recombine with the hydroperoxyl radical leading to the thio-(hydro)peroxy acid species through a barrierless process (see Figure S2).

Formation of NOS

Figure 4 presents a detailed map of the entire reaction pathway that was investigated. The kinetic barriers and thermodynamic ΔG values (kcal mol^{-1}) for all the relevant intermediates and side products are displayed herein. Departing from thio-(hydro)peroxy acid, two possible mechanisms for the formation of NOS are shown in Figure 5, namely the ionic and the radical pathways. The ionic pathway in (a) proceeds by transferring the hydroxyl group to the nitrogen, followed by a proton transfer to the oxygen bonded to the sulfur. This pathway was obtained by
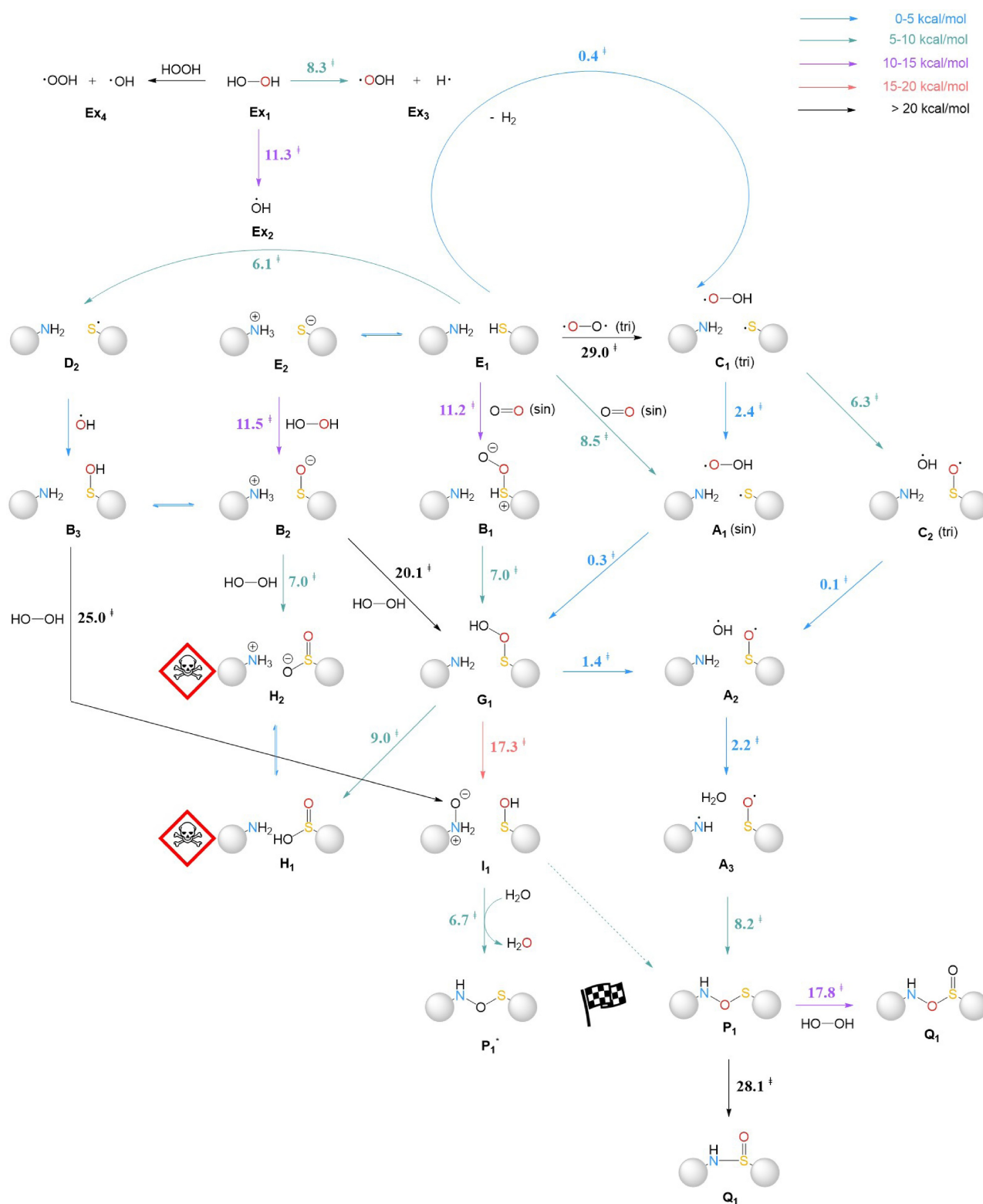
Figure 4. The computed reaction pathways between Cys and Lys in an oxidative environment, with the corresponding values represented in a water dielectric continuum. The dashed arrow from I_1 to P_1 reflects that the actual product is, located in the lower right corner, where the oxygen atom marked in red is released as water and the black one remains in NOS.

restricting the wave function to a closed-shell formalism. Then, a dehydration reaction takes place, removing the hydroxyl group from the newly formed sulfenic acid and one

proton from the amino oxide, with the assistance of an external water, leading to the NOS bridge formation. The fatal flaw of such pathway, however, is uncovered by
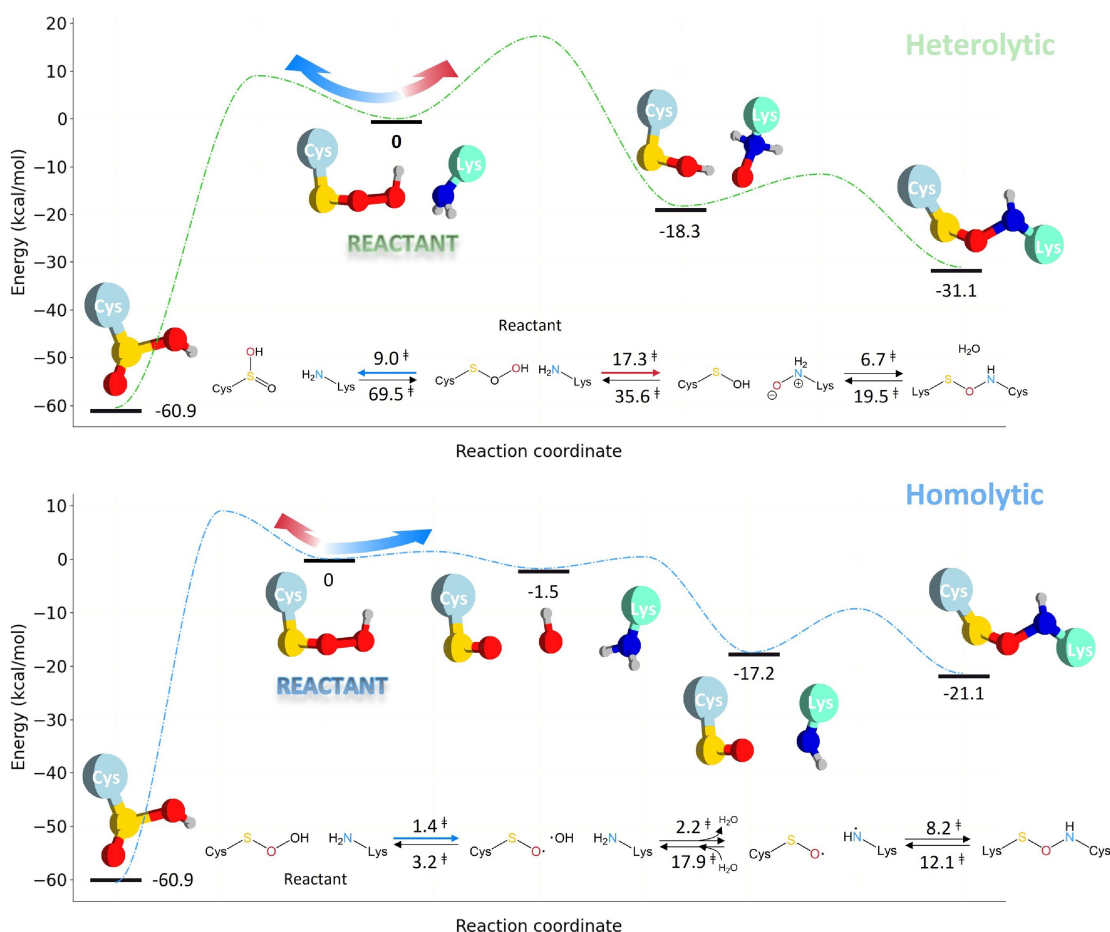
Figure 5. Energy diagram of NOS. The heterolytic and homolytic pathway corresponding to the dissociation of thio-(hydro)peroxy acid (computed without Lys).[62]

comparing the reaction barrier of transferring the hydroxyl group to the amine (17.3 kcal mol^{-1}) and to the sulfur (9.0 kcal mol^{-1}). The sulfinic acid is thereby the preferred product through the ionic pathway and virtually impossible to reverse due to its high stability. In contrast to the ionic pathway, the kinetic barrier for the homolytic dissociation of the O–O bond is merely 1.4 kcal mol^{-1}, enabling the system to avoid the formation of the sulfinic acid. A broken-symmetry solution was used for these calculations. The resulting hydroxyl radical can then easily strip a proton from the amine moiety with whom it was interacting, with a barrier of 2.2 kcal mol^{-1}, and form a radical species on the nitrogen atom of the Lys residue. Finally, the radical at the oxygen of the Cys residue and the nitrogen recombine, with an activation barrier of 8.2 kcal mol^{-1}, forming the NOS bond. An overview of all the involved reactions (and also other reaction possibilities which are not mentioned directly in the text) are given in Figure 4. Beside the advantage of avoiding sulfinic acid formation, another vital property of the homolytic dissociation pathway is its validity in expanding the NOS to the double-NOS (SONOS), sharing the same nitrogen.

Formation of SONOS

In M^{pro}, it was shown that a single NOS takes place with Cys22 and that further oxidation leads to the SONOS formation with Cys44.[6] In order to study the reaction mechanism for the double NOS formation and the preference for Cys22 or Cys44 herein, thermodynamic and kinetic results are presented (see Figure 6). Here we take the assumption that the oxidation of thiol to thio-(hydro)peroxy and its further homolytic dissociation are fairly similar for Cys22 and Cys44. The overall reaction mechanism which would differ regarding the involved Cys residue is then divided into two steps. In step (a), the H atom abstraction from the N atom by the newly formed •OH radical is studied. The kinetic barrier is slightly lower for the single NOS with Cys44, by about 4 kcal mol^{-1} and no difference is observed in the thermodynamic stability of the formed intermediate. However, the reactant state for the single NOS with Cys22 is thermodynamically favoured by 8 kcal mol^{-1}, which could potentiate its formation over the single NOS with Cys44. Step (b) corresponds to the recombination of the radicals leading to the SONOS formation. No significant differences are observed for the kinetic barriers so the preference for the single NOS
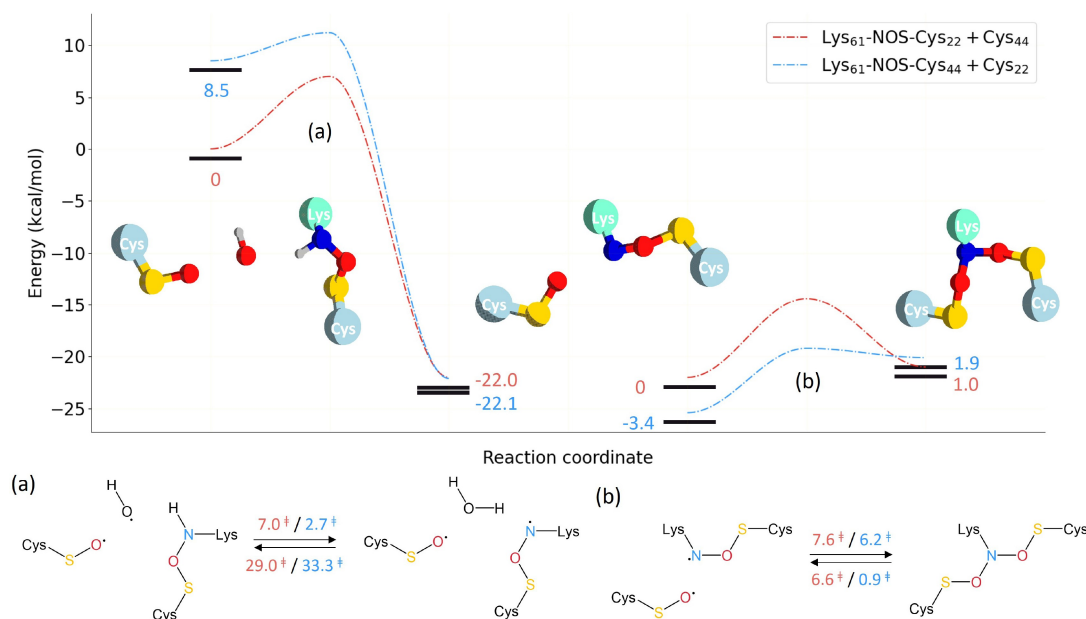
Figure 6. Energy diagram of SONOS. (a): The attack of •OH on the formed NOS. (b): The recombination of •O and •N. The energies and curves in red represent the situation where the NOS-bridge is first built by Lys61 with Cys22 and blue for the NOS-bridge formation with Cys44.[62]

formation with Cys22 is attributed to the relative reactant stability, or specific environment effects (e.g., exposure to solvent and oxidant species). In the case where two Cys residues are present, one also needs to consider the possibility of disulfide bond formation. In order for SONOS to be formed, the barrier for S–S formation needs to be somewhat higher. A well established reaction mechanism based on PBE50/6-311++G** calculations has been provided by Hagras et al.[63] using hydrogen peroxide as oxidant. A deprotonated Cys can be oxidised to sulfenic acid with a reaction barrier of 18.6 kcal mol^{-1} (11.3 kcal mol^{-1} from this work in Figure 2). The further cross-linking reaction forming the disulfide from sulfenic acid and thiol (the neighboring Cys) was reported to be 15.4 kcal mol^{-1}. The value is obtained with a microsolvation model, including two water molecules. We performed a conformer sampling using CREST2.11.1[64,65] for the transition state of this cross-linking step and optimized the conformers using the same level of theory as in the other reactions we are reporting (B3LYP–D3(BJ)/def2-TZVPD//B3LYP–D3(BJ)/def2-SVPD) followed by IRC-calculations. The reaction barriers for the 18 conformers found are distributed in the range of 8.9–12.5 kcal mol^{-1} (Figure 7), which is much lower than that from Hagras et al. with the Lys assisting the proton transfer. Averaging the conformers with their Boltzmann-factors and applying the conformational entropy correction (at 298.15 K) yields an effective reaction barrier of 10.7 kcal mol^{-1}. Removing the Lys residue and the constraints on the C$_\alpha$ atoms gives the general case for a disulfide bond formation, and the corresponding barriers lie in the range of 15.5–22.3 kcal mol^{-1}. The lowest barrier is in good agreement with the values obtained by Hagras et al.[63] In summary, the two Cys residues have to overcome a barrier of 11.3 kcal mol^{-1} (for the sulfenic acid formation) followed
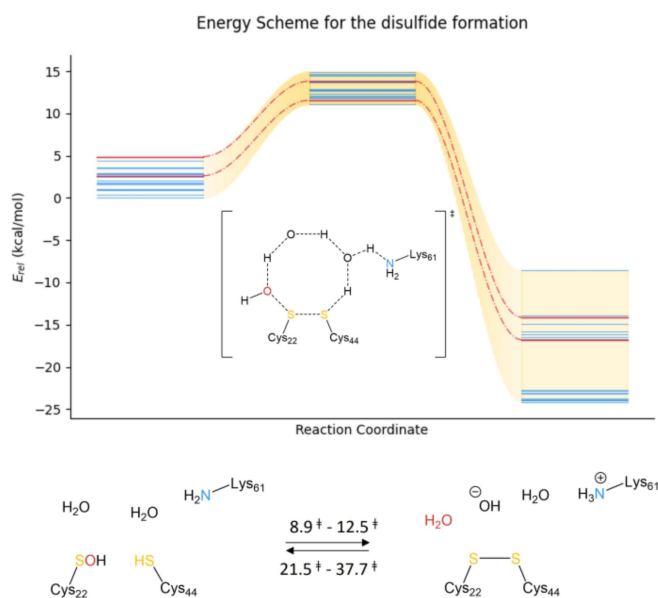

Figure 7. The computed energy diagram of the disulfide bond formation involving 18 conformers. The conformers with the lowest transition state barriers are represented by the red lines.

by a barrier of at least 8.9 kcal mol^{-1} to build the disulfide bond, both of which are higher than the largest barrier found on the way of forming SONOS (7.6 kcal mol^{-1} in Figure 6). Moreover, considering the extensive search we performed to find the lowest possible barrier for disulfide formation, there would be an overwhelming kinetic advantage for SONOS when two Cys residues are found in close proximity.

Conclusion

In the present work, the reaction mechanisms for the newly characterised single and double NOS bonds in proteins are computationally investigated. More than 30 reactions were considered for oxidation pathways involving different ROS. The results indicate that the sulfinic acid is thermodynamically very favoured and so its formation would lead the reaction to a dead end. An intermediate with a lower sulfur oxidation state is required for the formation of the NOS bond. The sulfenic acid is shown to be a suitable candidate but its overoxidation could potentially lead to the formation of the sulfinic acid. In this vein, the thio-(hydro)peroxy acid is shown to be another potential oxidation intermediate which allows the formation of the NOS bond. Several different oxidant agents are considered and it is shown that radical derivatives of H_2O_2 are readily able to form this intermediate. Redox potentials clearly show that the process should be reversible, which is further supported by the computed activation barriers. For the formation of the single NOS, the homolytic dissociation of thio-(hydro)peroxy acid is shown to be a likely step in the reaction mechanism, avoiding the formation of the thermodynamic trap, the sulfinic acid. The double NOS bond formation is then observed to take place through the same reaction mechanism, departing from an already formed single NOS bond and a readily oxidised Cys residue. This carries consequences for the one known system sporting a SONOS bridge, namely the main protease of SARS-CoV-2. The preference for the single NOS formation with Cys22 is concluded to occur due to higher thermodynamic stability of the reactant state, and could be involved in a conformational change in the second participating Cys.[6] The preference of forming SONOS against disulfide due to a thermodynamic stability is also demonstrated. Further work in our lab include examining the potential impact of the enzyme environment in the reported barriers (for a few selected systems). This work is exploratory, giving a broad perspective of the reactivity leading to NOS formation. The absolute barrier values should be taken with caution, given the model approach taken, and the use of DFT. Multireference effects will clearly affect the reaction barriers involving singlet oxygen, but also the relative barriers involving oxidation state changes to the sulfur atom should be taken with caution. Similar reactions studied in atmospheric chemistry[66] show that the level of theory can significantly impact the barriers. This involves, however, high-level wave function methods that do not allow for the broad scope intended in this work. We aim in the future to revisit individual steps of the presented reaction network and over time refine the data for kinetic modelling of the rich redox chemistry of Cys residues. Parallels to atmospheric chemistry would also be of interest, given that chains of electronegative atoms also form naturally under those conditions,[67] hinting at the role of partial desolvation and/or the locality of reaction sites.

Conflict of Interest

There are no conflict of interest to declare.

Data Availability Statement

The data that support the findings of this study are openly available in Göttingen Research Online Data at https://doi.org/10.25625/RCFQCG, reference number 20221128.

Keywords: NOS · Reaction Mechanisms · Reactive Oxygen Species · Disulfide bonds · Density Functional Theory

[1] C. E. Paulsen, K. S. Carroll, *Chem. Rev.* **2013**, *113*, 4633.

[2] D. Fass, *Annu. Rev. Biophys.* **2012**, *41*, 63.

[3] A. A. Dombkowski, K. Z. Sultana, D. B. Craig, *FEBS Lett.* **2014**, *588*, 206.

[4] J. T. McLean, A. Benny, M. D. Nolan, G. Swinand, E. M. Scanlan, *Chem. Soc. Rev.* **2021**, *50*, 10857.

[5] M. Wensien, F. R. von Pappenheim, L. M. Funk, P. Kloskowski, U. Curth, U. Diederichsen, J. Uranga, J. Ye, P. Fang, K. T. Pan, H. Urlaub, R. A. Mata, V. Sautner, K. Tittmann, *Nature* **2021**, *593*, 460.

[6] F. Rabe von Pappenheim, M. Wensien, J. Ye, J. Uranga, I. Irisarri, J. de Vries, L.-M. Funk, R. A. Mata, K. Tittmann, *Nat. Chem. Biol.* **2022**, *18*, 368.

[7] K. S. Yang, L. R. Blankenship, S.-T. A. Kuo, Y. J. Sheng, P. Li, C. A. Fierke, D. H. Russell, X. Yan, S. Xu, W. R. Liu, *ACS Chem. Biol.* **2023**, *18*, 449.

[8] D. Garrido Ruiz, A. Sandoval-Perez, A. V. Rangarajan, E. L. Gunderson, M. P. Jacobson, *Biochemistry* **2022**, *61*, 2165.

[9] Z. Wang, J. D. Rabb, Q. Lin, *Chem. Eur. J.* **2023**, *29*, e202202828.

[10] H. Feng, Q. Zhao, B. Zhang, H. Hu, M. Liu, K. Wu, X. Li, X. Zhang, L. Zhang, Y. Liu, *Angew. Chem. Int. Ed.* **2023**, *62*, e202215215.

[11] J. Nakamura, J. R. Purvis, J. A. Swenberg, *Nucleic Acids Res.* **2003**, *31*, 1790.

[12] K. Tittmann, L.-M. Funk, F. R. von Pappenheim, M. Wensien, N. Eulig, E. Penka, K. Stegmann, A. Dickmanns, M. Dobbelstein, R. Mata, J. Uranga, S. Bazzi, T. Fritz, A. Chari, E. Paknia, G. Heyne, A. Pearson, R. Hilgenfeld, U. Curth, C. Berndt, G. Poschmann, Multiple redox switches of the SARS-CoV-2 main protease in vitro provide new opportunities for drug design, **2022**.

[13] S. Carballal, B. Alvarez, L. Turell, H. Botti, B. a Freeman, R. Radi, *Amino Acids* **2007**, *32*, 543.

[14] A. Galano, *Theor. Chem. Acc.* **2011**, *130*, 51.

[15] *Oxidative Stress and Redox Regulation* (Eds.: U. Jakob, D. Reichmann), Springer, Netherlands, **2013**.

[16] A. Zeida, C. M. Guardia, P. Lichtig, L. L. Perissinotti, L. A. Defelipe, A. Turjanski, R. Radi, M. Trujillo, D. A. Estrin, *Biophys. Rev. Lett.* **2014**, *6*, 27.

[17] J. Uranga, J. I. Mujika, J. M. Matxain, *J. Phys. Chem. B* **2015**, *119*, 15430.

[18] L. J. Alcock, M. V. Perkins, J. M. Chalker, *Chem. Soc. Rev.* **2018**, *47*, 231.

[19] G. Roos, J. Messens, *Free Radical Biol. Med.* **2011**, *51*, 314.

[20] S. Reina, M. G. G. Pittalà, F. Guarino, A. Messina, V. De Pinto, S. Foti, R. Saletti, *Front. Cell Dev. Biol.* **2020**, *8*.

[21] R. Franco, J. A. Cidlowski, *Cell Death Differ.* **2009**, *16*, 1303.

[22] A. Amici, R. L. Levine, L. Tsai, E. R. Stadtman, *J. Biol. Chem.* **1989**, *264*, 3341.

[23] N. Chondrogianni, I. Petropoulos, S. Grimm, K. Georgila, B. Catalgol, B. Friguet, T. Grune, E. S. Gonos, *Mol. Aspects Med.* **2014**, *35*, 1.

[24] J. Uranga, J. I. Mujika, R. Grande-Aztatzi, J. M. Matxain, *J. Phys. Chem. B* **2018**, *122*, 4956.

[25] M. Ruszkowski, Z. Dauter, *Protein Sci.* **2016**, *25*, 1734.

[26] M. Ruszkowski, Z. Dauter, *Protein Sci.* **2019**, *28*, 470.

[27] J. Wang, *Protein Sci.* **2019**, *28*, 472.

[28] B. W. Matthews, *Protein Sci.* **2021**, *30*, 1491.

[29] H. Sies, V. V. Belousov, N. S. Chandel, M. J. Davies, D. P. Jones, G. E. Mann, M. P. Murphy, M. Yamamoto, C. Winterbourn, *Nat. Rev. Mol. Cell Biol.* **2022**, *23*, 499.

[30] K. Krumova, G. Cosa, in *Singlet Oxygen: Applications in Biosciences and Nanosciences, Vol. 1*, The Royal Society of Chemistry, Cambridge, **2016**, Chapter 1 Overview of Reactive Oxygen Species, pp. 1–21.

[31] J. K. Lee, K. L. Walker, H. S. Han, J. Kang, F. B. Prinz, R. M. Waymouth, H. G. Nam, R. N. Zare, *Proc. Natl. Acad. Sci. USA* **2019**, *116*, 19294.

[32] E. A. Veal, A. M. Day, B. A. Morgan, *Mol. Cell* **2007**, *26*, 1.

[33] J. Krasnovsky, *Biochemistry* **2007**, *72*.

[34] J. I. Mujika, J. Uranga, J. M. Matxain, *Chem. Eur. J.* **2013**, *19*, 6862.

[35] J. Uranga, O. Lakuntza, E. Ramos-Cordoba, J. M. Matxain, J. I. Mujika, *Phys. Chem. Chem. Phys.* **2016**, *18*, 30972.

[36] R. D. Bach, P. Y. Ayala, H. B. Schlegel, *J. Am. Chem. Soc.* **1996**, *118*, 12758.

[37] T. Autrey, A. K. Brown, D. M. Camaioni, M. Dupuis, N. S. Foster, A. Getty, *J. Am. Chem. Soc.* **2004**, *126*, 3680.

[38] D. Hieu C, H. Thi H, N. Thu M, K. Yoshiyuki, L. Hung M, *J. Comput. Chem.* **2021**, *42*, 1344.

[39] D. Fass, S. Semenov, *Nature* **2021**, *593*, 343.

[40] X. Zhu, P. Li, Q. Shi, L. Wang, *Green Chem.* **2016**, *18*, 6373.

[41] Z. Yang, X. Song, Z. Wei, J. Cao, D. Liang, H. Duan, Y. Lin, *Tetrahedron Lett.* **2016**, *57*, 2410.

[42] M. J. Frisch, G. W. Trucks, H. B. Schlegel, G. E. Scuseria, M. A. Robb, J. R. Cheeseman, G. Scalmani, V. Barone, G. A. Petersson, H. Nakatsuji, X. Li, M. Caricato, A. V. Marenich, J. Bloino, B. G. Janesko, R. Gomperts, B. Mennucci, H. P. Hratchian, J. V. Ortiz, A. F. Izmaylov, J. L. Sonnenberg, D. Williams-Young, F. Ding, F. Lipparini, F. Egidi, J. Goings, B. Peng, A. Petrone, T. Henderson, D. Ranasinghe, V. G. Zakrzewski, J. Gao, N. Rega, G. Zheng, W. Liang, M. Hada, M. Ehara, K. Toyota, R. Fukuda, J. Hasegawa, M. Ishida, T. Nakajima, Y. Honda, O. Kitao, H. Nakai, T. Vreven, K. Throssell, J. A. Montgomery, Jr, J. E. Peralta, F. Ogliaro, M. J. Bearpark, J. J. Heyd, E. N. Brothers, K. N. Kudin, V. N. Staroverov, T. A. Keith, R. Kobayashi, J. Normand, K. Raghavachari, A. P. Rendell, J. C. Burant, S. S. Iyengar, J. Tomasi, M. Cossi, J. M. Millam, M. Klene, C. Adamo, R. Cammi, J. W. Ochterski, R. L. Martin, K. Morokuma, O. Farkas, J. B. Foresman, D. J. Fox, Gaussian16 Revision A.03 **2016**, gaussian Inc. Wallingford CT.

[43] A. D. Becke, *J. Chem. Phys.* **1992**, *96*, 2155.

[44] C. Lee, W. Yang, R. G. Parr, *Phys. Rev. B* **1988**, *37*, 785.

[45] F. Weigend, R. Ahlrichs, *Phys. Chem. Chem. Phys.* **2005**, *7*, 3297.

[46] F. Weigend, *Phys. Chem. Chem. Phys.* **2006**, *8*, 1057.

[47] S. Grimme, J. Antony, S. Ehrlich, H. Krieg, *J. Chem. Phys.* **2010**, *132*, 154104.

[48] S. Grimme, S. Ehrlich, L. Goerigk, *J. Comput. Chem.* **2011**, *32*, 1456.

[49] A. V. Marenich, C. J. Cramer, D. G. Truhlar, *J. Phys. Chem. B* **2009**, *113*, 6378.

[50] O. Weser, B. Hein-Janke, R. A. Mata, *J. Comput. Chem.* **2023**, *44*, 710.

[51] G. Luchini, J. Alegre-Requena, I. Funes-Ardoiz, R. Paton, *F1000Research* **2020**, *9*.

[52] S. Grimme, *Chem. Eur. J.* **2012**, *18*, 9955.

[53] T. Lu, F. Chen, *J. Comput. Chem.* **2012**, *33*, 580.

[54] F. L. Hirshfeld, *Theor. Chim. Acta* **1977**, *44*, 129.

[55] A. D. Becke, *J. Chem. Phys.* **1988**, *88*, 2547.

[56] I. Mayer, P. Salvador, *Chem. Phys. Lett.* **2004**, *383*, 368.

[57] G. Shields, P. Seybold, *Computational Approaches to Predict pKa Values*, CRC Press, Boca Raton, **2014**.

[58] W. Jeong, S. J. Park, T.-S. Chang, D.-Y. Lee, S. G. Rhee, *J. Biol. Chem.* **2006**, *281*, 14400.

[59] P. R. Ogilby, *Chem. Soc. Rev.* **2010**, *39*, 3181.

[60] M. Hayyan, M. A. Hashim, I. M. AlNashef, *Chem. Rev.* **2016**, *116*, 3029.

[61] J. W. Mullinax, C. W. Bauschlicher, J. W. Lawson, *J. Phys. Chem. A* **2021**, *125*, 2876.

[62] G. Schaftenaar, J. Noordik, *J. Comput.-Aided Mol. Des.* **2000**, *14*, 123.

[63] M. A. Hagras, M. A. Bellucci, G. Gobbo, R. A. Marek, B. L. Trout, *J. Phys. Chem. B* **2020**, *124*, 9840.

[64] S. Grimme, *Phys. Chem. Chem. Phys.* **2019**, *15*, 2847.

[65] P. Pracht, F. Bohle, S. Grimme, *J. Chem. Theory Comput.* **2020**, *22*, 7169.

[66] J. Chen, T. Berndt, K. H. Møller, J. R. Lane, H. G. Kjaergaard, *J. Phys. Chem. A* **2021**, *125*, 8933.

[67] T. Berndt, J. Chen, E. R. Kjærgaard, K. H. Møller, A. Tilgner, E. H. Hoffmann, H. Herrmann, J. D. Crounse, P. O. Wennberg, H. G. Kjaergaard, *Science* **2022**, *376*, 979.